Inorganic Chemistry

Article

pubs.acs.org/IC

Triple-Emitting Dumbbell Fluorescent Nanoprobe for Multicolor Detection and Imaging Applications

Jing Liu,[†] Jian Liu,[†] Weisheng Liu,[†] Haoli Zhang,[†] Zhengyin Yang,[†] Baodui Wang,*[,†] Fengjuan Chen,[†] and Haotai Chen*[,‡]

[†]Key Laboratory of Nonferrous Metal Chemistry and Resources Utilization of Gansu Province, State Key Laboratory of Applied Organic Chemistry, and Key Laboratory of Special Function Materials and Structure Design, Ministry of Education, Lanzhou University Gansu, Lanzhou, 730000, P. R. China

[‡]State Key Laboratory of Veterinary Etiologic Biology, National Foot-and-Mouth Disease Reference Laboratory of China, Lanzhou Veterinary Research Institute, Chinese Academy of Agricultural Sciences, Lanzhou, 730046, Gansu, P. R. China

Supporting Information

ABSTRACT: The combination of different fluorescent species into one nanostructure to develop fluorescent nanoparticles with multiple emission signatures by a single wavelength excitation has become a very popular research area in the field of multiplex bioanalysis, diagnostics, and multicolor imaging. However, these novel hybrids must be elaborately designed to ensure that the unique properties of each component are conveyed, i.e., fluorescent species and nanoparticles, and are maximized without serious interactions with each other. Herein, a first triple-fluorescence dumbbell nanoprobe with large Stokes shift based on incorporating fluorescein isothiocyanate (FITC) and lanthanide complexes onto Au−Fe_3O_4 NPs was synthesized. This hybrid displays well-resolved triple fluorescence emission, with FITC at 515 nm, Tb(III) complex at 545 nm, and Eu(III) complex at 616 nm under a single-excitation wavelength and is used for highly selective and sensitive colorimetric detection of Cu^{2+} with a detection limit of 30 nM. Under different Cu^{2+} concentrations, this hybrid exhibited distinguishable multiple colors under UV light, and the color could change in the presence of different concentrations of Cu^{2+}. This sensor for ratio/multianalyte microscopic imaging of Cu^{2+} in HeLa cells and BHK cells was also demonstrated. Target molecules, such as folic acid, can be covalently attached to the fluorescent nanoparticle surface to serve as an effective probe for simultaneous multicolor imaging folate receptor-overexpressing HeLa cell lines in vitro.

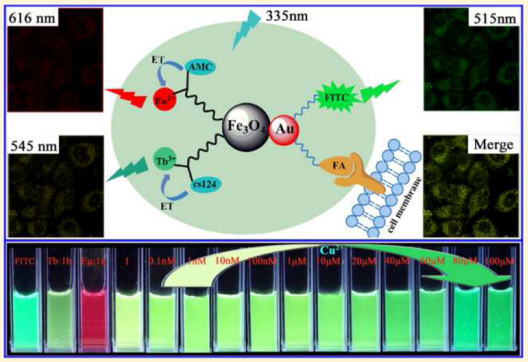

INTRODUCTION

Integrating different kinds of fluorescent species into one nanostructure is an attractive way to develop encoding fluorescent nanoprobes for simultaneous multicolor imaging, multiplex bioassays, and diagnostics without complex instrumentation and processing.[1−9] Organic dyes and luminescent lanthanide complexes are typical fluorescent materials, which have been incorporated into various nanosized matrixes, such as silica,[10−13] Au nanoparticles (NPs),[14−18] and magnetic nanoparticles[19−23] for high capacity spectral encoding. Organic-dye-incorporated nanoparticles emit a strong fluorescence signal and exhibit highly enhanced photostability, which makes them particularly suitable for ultrasensitive bioassay. However, the number of available organic dyes with the same excitation and different emission is limited, which restricts the number of distinctly spectral codes that can be produced.[7,24,25] Lanthanide complexes have attracted intense interest due to their special photophysical properties of large Stokes shift, narrow emission bands, high quantum yields, and long luminescence lifetimes.[26−29] These unique optical properties provide a significant signal-to-noise ratio enhancement compared to that of conventional organic fluorophores.[30,31] Although organic dyes and lanthanide-based complexes have been broadly studied for biomedical applications, integrating organic dye, Tb(III) complex, and Eu(III) complex on magnetic NPs has never been synthesized and studied. Such conjugates with different kinds of fluorescent species based on the different emission behaviors of fluorescein isothiocyanate (FITC) (515 nm), Tb(III) complex (545 nm), and Eu(III) complex (616 nm) by a single wavelength excitation should serve as promising multianalyte fluorescence sensors and multicolor imaging agents for generating interesting behavior and functionalities far beyond those of their individual species.

On the other hand, as scaffolds for preparing the multifunctional nanoprobe, the dumbbell structure Au−Fe_3O_4 NPs have attracted much attention. Such NPs contain both Au and Fe_3O_4 NPs, which are known to be biocompatible and have been widely used for optical and magnetic applications in biomedicine.[23,32,33] Furthermore, compared with other single-

Received: March 17, 2015
Published: August 3, 2015

DOI: 10.1021/acs.inorgchem.5b00610
Inorg. Chem. 2015, 54, 7725−7734

Scheme 1. Synthetic Route of 1 and 3

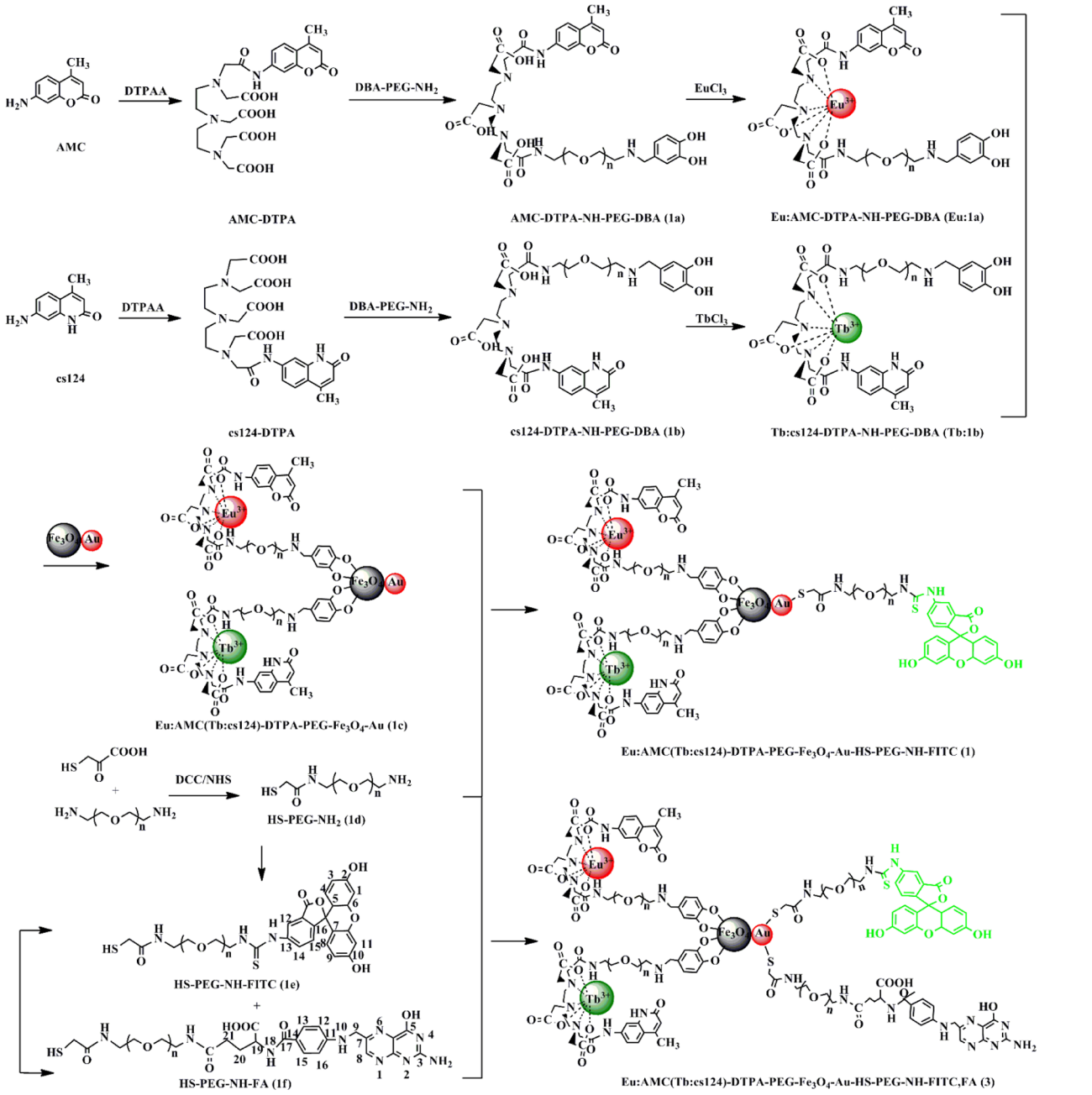

component NPs and other core/shell Fe_3O_4/Au NPs,[34] such NPs could provide two functional surfaces for binding different kinds of molecules for ratiometric detection and magnetic separation applications.

On the other hand, the development of efficient methods for highly sensitive, fast, and accurate detection of metal ions and various target analytes in vitro or in vivo is essential for the early diagnosis of serious diseases. Copper is a commonly used metal that can leak into the environment through various means. Low concentration of copper is an essential nutrient. However, excessive copper ions are toxic and can lead to many serious human afflictions,[35] both acutely and chronically. Therefore, the monitoring of Cu^{2+} in biological and environmental systems is highly important. Recently, several lanthanide sensors for Cu^{2+} have been developed.[36,37] However, most of these sensors detect copper ions by enhancing or quenching the single emission intensity.

In this work, we report a unique hybrid dumbbell-like structure that comprises FITC, Tb:**1b**,[19] and Eu:**1a**[21] grafted onto the surface of Au−Fe_3O_4 NPs (Scheme 1). This hybrid (**1**) exhibits a single-excitation, triple-emission fluorescence property, two from the Tb(III) complex and Eu(III) complex with green and red emission colors, respectively, and the other from the FITC acting as a reference. This above phenomenon was attributed to the large Stokes shift and the sharp emission of lanthanide chelates,[39,40] as well as the appropriate matching in the excitation wavelength of FITC, Tb(III) complex, and Eu(III) complex, which is different from previously reported nanoparticles that show single excitation and overlapped emission,[7,24,25,38,39] thereby creating ideal conditions for multiple detection without any spectroscopic distortion. We

DOI: 10.1021/acs.inorgchem.5b00610
Inorg. Chem. 2015, 54, 7725−7734

demonstrated that DTPA-cs124 and DTPA-AMC have a higher binding constant for Cu^{2+} ($K_{Cu:DTPA-cs124} = 10^{22.26}$ and $K_{Cu:DTPA-AMC} = 10^{21.77}$) than Tb^{3+} ($K_{Tb:DTPA-cs124} = 10^{20.44}$) and Eu^{3+} ($K_{Eu:DTPA-AMC} = 10^{19.67}$) (Supporting Information Figures S1 and S2, Tables 1 and 2). Consequently, in the presence of Cu^{2+}, Tb^{3+} and Eu^{3+} can be replaced by Cu^{2+} to form Cu:DTPA-cs124 and Cu:DTPA-AMC, resulting in fluorescent quenching of **1** (Scheme 2). So, **1** exhibited distinguishable multicolor fluorescence with different concentrations of Cu^{2+} ions, which extend their use in multiple imaging applications. Moreover, folic-acid-labled **1** enables targeted multiple fluorescent imaging of folate receptor (FR)-overexpressing HeLa cell lines in vitro.

Table 1. Protonation Constants of Ligands

ligand	K_1^H	K_2^H	K_3^H	K_4^H
DTPA-cs124	$10^{6.98}$	$10^{5.34}$	$10^{4.21}$	$10^{3.82}$
DTPA-AMC	$10^{6.42}$	$10^{5.01}$	$10^{4.14}$	$10^{3.81}$

Table 2. Stability Constants of Complexes

complex	K_1	K_2	K_3	K_4	K
Tb:DTPA-cs124	$10^{4.01}$	$10^{4.62}$	$10^{5.68}$	$10^{6.13}$	$10^{20.44}$
Cu:DTPA-cs124	$10^{4.06}$	$10^{5.23}$	$10^{6.21}$	$10^{6.76}$	$10^{22.26}$
Eu:DTPA-AMC	$10^{3.91}$	$10^{4.29}$	$10^{5.52}$	$10^{5.95}$	$10^{19.67}$
Cu:DTPA-AMC	$10^{3.96}$	$10^{4.43}$	$10^{6.43}$	$10^{6.95}$	$10^{21.77}$

EXPERIMENTAL SECTION

Materials. $HAuCl_4 \cdot 3H_2O$, *tert*-butylamine-borane (TBAB), oleylamine, oleic acid, 1,2,3,4-tetrahydronaphthalene (tetralin), 1-octadecene, $Fe(CO)_5$, 3,4-dihydroxybenzaldehyde, 7-amino-4-methyl coumarin (AMC), 7-amino-4-methyl-2(1*H*)-quinolinone (carbostyril 124, cs124), polyethylene glycol (M_W = 2000 and 4000), and fluorescein isothiocyanate (FITC) were purchased from Sigma-Aldrich. Folic acid (FA), thioglycollic acid, dicyclohexylcarbodiimide (DCC), and *N*-hydroxysuccinimide (NHS) were from Aladdin in China. Au−Fe_3O_4 nanoparticles,[41] diethylenetriaminepentaacetic acid dianhydride[42] (DTPAA), 1,ω-diaminopolyoxyethylene[43] (NH_2-PEG-NH_2, M_W = 2000 and 4000), polyethylene glycol 3,4-dihydroxybenzylamine[19] (H_2N-PEG-DBA, M_W = 4000), HS-PEG-NH_2[23] (M_W = 2000), HS-PEG-NH-FITC[23] (M_W = 2000), HS-PEG-NH-FA[23] (M_W = 2000), Tb:cs124-DTPA-NH-PEG-DBA (Tb:**1b**),[19] and Eu:AMC-DTPA-NH-PEG-DBA (Eu:**1a**)[21] were prepared according to previous work. The stock solutions of metal ions were prepared in double distilled water (ddH_2O) by using corresponding salts ($CuCl_2$, $FeSO_4$, $Hg(ClO_4)_2$, KNO_3, $NaNO_3$, $Zn(NO_3)_2$, $Mg(NO_3)_2$, $Ca(NO_3)_2$, $Ni(NO_3)_2$, $Cd(NO_3)_2$, $BaCl_2$, $Pb(OAc)_2$, $FeCl_3$, $Co(NO_3)_2$, $Mn(OAc)_2$, $Cu(CH_3COO)_2$, $CuSO_4$, $Cu(NO_3)_2$). The pH value and ionic strength in all aqueous solutions were maintained through Tris-HCl (50 mM, NaCl 50 mM, pH 7.20) buffer. All chemicals were directly used without further purification, except DMF, $CHCl_3$, and triethylamine were redistilled. $EuCl_3 \cdot 6H_2O$ and $TbCl_3 \cdot 6H_2O$ were obtained by dissolving Eu_2O_3 and Tb_4O_7 in diluted HCl, followed by removing excess amounts of acid, and Tb_4O_7 aqueous species were oxidated to $TbCl_3$ by adding H_2O_2.

Measurements. The TEM images were obtained on Philips EM 420 (120 kV). The fluorescence spectra were obtained from the Shimadzu RF-5301 spectrofluorophotometer. The fluorescence lifetimes were performed on the FLS920 steady state−transient state fluorescence spectrometer. The magnetization was carried out on a Lake Shore 7400 VSM system at 300 K. Dynamic light scattering and zeta potential experiments were performed with a Malvern Zetasizer Nano ZS90 laser diffraction particle size analyzer, and the sample was measured three times; the particle size (hydrodynamic diameter) and zeta potential were averaged. FT-IR characterization was carried out on a Bruker Vertex 70 FT-IR spectrometer. ^1H NMR spectra were acquired with a Varian 400 MHz NMR. UV−vis absorbance measurements were recorded on Shimadzu UV-1750. Fluorescent images were got from Leica TCS SP8 inverted epifluorescence/reflectance laser scanning confocal microscope.

Synthesis of Au−Fe_3O_4 Nanoparticles. Au−Fe_3O_4 NPs were prepared according to our previous work.[41] A 20 mg portion of Au NPs as seeds in oleylamine (2 mL) were dispersed in a solution of 1-octadecene (20 mL) and oleic acid (1 mL). The solution was stirred under a mild flow of nitrogen at 120 °C for 1 h. Then, under a blanket of nitrogen, $Fe(CO)_5$ (0.10 mL) was injected into the above solution. The reaction solution was heated to 300 °C and refluxed for 25 min. After cooling to room temperature, the Au−Fe_3O_4 particles were precipitated by adding isopropanol (40 mL) and then separated by centrifugation. The formed Au−Fe_3O_4 NPs were redispersed into hexane.

Synthesis of AMC-DTPA-NH-PEG-DBA (1a) and cs124-DTPA-NH-PEG-DBA (1b). For the synthesis of AMC-DTPA-NH-PEG-DBA (**1a**), a solution of AMC (17.5 mg, 0.1 mmol) in anhydrous DMF (5 mL) was added dropwise into the suspension of DTPAA (35.7 mg, 0.1 mmol) in DMF (5 mL) and dry triethylamine (100 μL) within 30 min at 25 °C. After the mixture solution became clear, DBA-PEG-NH_2 (400 mg, 0.1 mmol) in anhydrous $CHCl_3$ (10 mL) was added dropwise within 10 min, and the mixture continued to stir for 12 h. Diethyl ether was added into the solution, and then the precipitate was collected by centrifugation. After washing with DMF, CH_2Cl_2, and diethyl ether, the product was then dried under vacuum. DTPA-AMC: ESI-MS, m/z = 550.4, $[M + H]^+$. AMC-DTPA-NH-PEG-DBA ^1H NMR (d_6-DMSO, 400 MHz), δ ppm: 2.43 (s, 3H, $—CH_{3DTPA-AMC}$), 2.98 (t, 8H, $CH_2—N_{DTPA-AMC}$), 3.35 (s, 10H, $CH_2—C{=}O_{DTPA-AMC}$), 3.43 (s, 2H, $CH_2—NH_{DBA-PEG-NH}$), 3.53 (bs, ~360H, PEG4000), 6.12 (s, 1H, $Ph_{DTPA-AMC}$), 6.28 (s, 1H, $Ph_{DBA-PEG-NH}$), 6.76 (d, 1H, $Ph_{DBA-PEG-NH}$), 6.99 (d, 1H, $Ph_{DBA-PEG-NH}$), 7.30 (d, 1H, $Ph_{DTPA-AMC}$), 7.76 (d, 1H, $Ph_{DTPA-AMC}$), 8.00 (s, 1H, $Ph_{DTPA-AMC}$).

Scheme 2. Schematic Description of Cu^{2+} Detection

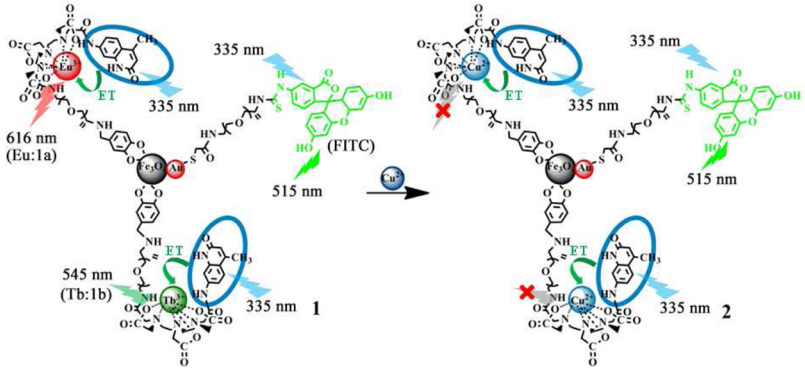

DOI: 10.1021/acs.inorgchem.5b00610
Inorg. Chem. 2015, 54, 7725−7734

Under similar reaction conditions, cs124-DTPA-NH-PEG-DBA (**1b**) was also synthesized by using DTPAA (35.7 mg, 0.1 mmol), cs124 (17.4 mg, 0.1 mmol), and DBA-PEG-NH_2 (0.4 g, 0.1 mmol). DTPA-cs124: ESI-MS, m/z = 551.3, $[M + H]^+$. cs124-DTPA-NH-PEG-DBA ^{1}H NMR (d_6-DMSO, 400 MHz), δ ppm: 2.38 (s, 3H, —$CH_{3DTPA\text{-}cs124}$), 2.98 (t, 8H, CH_2—$N_{DTPA\text{-}cs124}$), 3.34 (s, 10H, CH_2—C═$O_{DTPA\text{-}cs124}$), 3.41 (s, 2H, CH_2—$NH_{DBA\text{-}PEG\text{-}NH}$), 3.51 (bs, ∼360H, PEG4000), 6.18 (s, 1H, $Ph_{DTPA\text{-}cs124}$), 6.24 (s, 1H, $Ph_{DBA\text{-}PEG\text{-}NH}$), 6.76 (d, 1H, $Ph_{DBA\text{-}PEG\text{-}NH}$), 6.95 (d, 1H, $Ph_{DBA\text{-}PEG\text{-}NH}$), 7.32 (s, 1H, $Ph_{DTPA\text{-}cs124}$), 7.45 (d, 1H, $Ph_{DTPA\text{-}cs124}$), 8.00 (d, 1H, $Ph_{DTPA\text{-}cs124}$)

Synthesis of Eu:AMC-DTPA-NH-PEG-DBA (Eu:1a) and Tb:cs124-DTPA-NH-PEG-DBA (Tb:1b). $TbCl_3{\cdot}6H_2O$ (37.4 mg, 0.1 mmol) and $EuCl_3{\cdot}6H_2O$ (36.7 mg, 0.1 mmol) were added into the DMF solution containing 0.1 mmol of **1a** and 0.1 mmol of **1b**, respectively, and stirred for 12 h at 25 °C. Diethyl ether was added into the solution, and then the precipitate was collected by centrifugation. After being washed with DMF, CH_2Cl_2, and diethyl ether, the product was then dried under vacuum.

Synthesis of Eu:AMC(Tb:cs124)-DTPA-PEG-Fe_3O_4-Au (1c). Au−Fe_3O_4 (10 mL $CHCl_3$) was added into the DMF (3 mL) solution containing **Eu:1a** (48.4 mg, 10 μmol) and **Tb:1b** (8.2 mg, 1.7 μmol). The mixture was stirred for 24 h at 25 °C. Diethyl ether was added into the solution, and then the precipitate was collected by centrifugation. After being washed with DMF, ethanol, and petroleum ether, the product was then redispersed in $CHCl_3$.

Synthesis of HS-PEG-NH_2 (1d). To a solution of thioglycollic acid (9.2 mg, 0.1 mmol) in dry DMF (2 mL) was added DCC (31 mg, 0.15 mmol) and NHS (14 mg, 0.12 mmol). After the mixture was stirred at 25 °C for 24 h in the dark, the white precipitate was discarded by centrifugation. The filtrate was mixed with poly(ethylene glycol)bis-(amine) (0.2 g, 0.1 mmol, M_W = 2000) in 10 mL of CH_2Cl_2 and allowed to react at 25 °C for 12 h. The solvent was concentrated under reduced pressure, precipitated with diethyl ether, and then dried under vacuum. ^{1}H NMR ($CDCl_3$, 400 MHz), δ ppm: 3.82 (s, 2H, $SHCH_2$), 3.65 (bs, ∼180H, PEG 2000), 3.50 (t, 2H, $NH_2CH_2CH_2$), 3.47 (t, 2H, CH_2NH_2).

Synthesis of HS-PEG-NH-FITC (1e). FITC (3.9 mg, 10.0 μmol) and **1d** (21.0 mg, 11.0 μmol) were dissolved in ethanol (2 mL) and $CHCl_3$ (2 mL) at 25 °C and stirred in the dark for 4 h. Diethyl ether was added into the solution, and then, the precipitate was collected by centrifugation. After being washed with DMF, CH_2Cl_2, and diethyl ether, the product was then dried under vacuum. ^{1}H NMR ($CDCl_3$, 400 MHz), δ ppm: 7.39 (m, 3H, C12, C13, C14), 6.42−6.80 (m, 6H, C1, C3, C4, C8, C9, C11), 3.81 (s, 2H, $SHCH_2$), 3.77 (d, 2H, C5, C6), 3.64 (bs, ∼180H, PEG 2000), 3.50 (t, 2H, $NHCH_2CH_2$), 3.45 (t, 2H, $NHCH_2$).

Synthesis of HS-PEG-NH-FA (1f). Folic acid (4.4 mg, 10 μmol) was dissolved in dry DMSO (2 mL), and then DCC (3.1 mg, 15 μmol) and NHS (1.4 mg, 12 μmol) were added. The reaction mixture was stirred for 12 h at room temperature in the dark. The byproduct, dicyclohexylurea, was filtered off. The filtrate was mixed with **1d** (21.0 mg, 11.0 μmol) and allowed to react at 25 °C for 12 h. Diethyl ether was added into the solution, and then the precipitate was collected by centrifugation. After being washed with DMF, CH_2Cl_2, and diethyl ether, the product was then dried under vacuum. ^{1}H NMR (DMSO, 400 MHz), δ ppm: 8.65 (s, 1H, C8), 7.63 (d, 2H, C13, C15), 6.64 (d, 2H, C12, C16), 4.48 (s, 2H, C9), 4.30 (t, H, C19), 4.16 (t, 2H, $HSCH_2$), 3.25 (t, 2H, $NHCH_2CH_2$), 3.51 (bs, ∼180H, PEG 2000), 3.20 (t, 2H, $NHCH_2$), 2.29 (t, 2H, C21), 1.90 (m, 2H, C20).

Synthesis of Eu:AMC(Tb:cs124)-DTPA-PEG-Fe_3O_4-Au-HS-PEG-NH-FITC (1). **1e** (4.9 mg, 2.0 μmol) was added into the solution of **1c** and stirred for 6 h in the dark at 25 °C. After petroleum ether was added to the reaction solution, the obtained solid was collected by centrifugation, dispersed in water, and dialyzed with H_2O for 24 h to remove the free **1e**.

Synthesis of Eu:AMC(Tb:cs124)-DTPA-PEG-Fe_3O_4-Au-HS-PEG-NH-FITC,FA (3). **1e** (4.9 mg, 2.0 μmol) and **1f** (4.8 mg, 2.0 μmol) were dissolved in $CHCl_3$ (3 mL), and then **1c** (10 mg) in $CHCl_3$ (10 mL) was added. The mixture was stirred at 25 °C for 24 h. After petroleum ether was added and the material centrifuged, the product was then redispersed in H_2O.

Potentiometric Studies. The protonation constants of the ligands (DTPA-cs124 and DTPA-AMC) and the stability constants (binding constrants) of the complexes (Tb:DTPA-cs124, Cu:DTPA-cs124, Eu:DTPA-AMC, and Cu:DTPA-AMC) were studied in 0.10 mol dm^{-3} NaCl aqueous soultion at 25 °C using potentiometric pH titration method. The protonation constants of ligands were first calculated and used for determining the stability constants of the complexes. The each potentiometric measurement was performed by titration in 50 mL NaCl aqueous solution with standard NaOH solutions. All solutions used in potentiometric studies are as follows: (a) ligands (10 mL, 1 mM) + NaCl (50 mL, 0.1 M) for the determination of the protonation constants of the ligands, (b) ligands (10 mL, 1 mM) + metal ions (10 mL, 1 mM) + NaCl (50 mL, 0.1 M) for the determination of the stability constants of the complexes. The computations of protonation constants of ligands and the stability constants of complexes were calculated using Bjerrum's Half-$\bar{n}$ Method.[44] All of the potentiometric data were collected between pH 3.0 and 10.0.

Detection of Cu^{2+}. A stock solution of **1** (1 mM Eu^{3+}, 0.1 mM Tb^{3+}) was measured by ICP-AES in double distilled water (ddH_2O). The aqueous solution of **1** was then diluted with Tris-HCl buffer (50 mM, pH 7.20, 50 mM NaCl) for the fluorescence detection of Cu^{2+} and other selected metal ions. The color change was observed under excitation at UV light.

Cytotoxicity Assay. In vitro cytotoxicity of **1** was evaluated by performing MTT assay of the BHK-21 cells and HeLa cells incubated with the particles. Cells with a density of 5 × 10^4 cells/well were seeded into a 96-well cell culture plate in DMEM (Dulbecco's modified eagle's medium) with 10% FBS (fetal bovine serum) at 37 °C under 5% CO_2 for 24 h. Then, the cells were incubated with different concentrations of **1** (4, 40, 140, 180 μM Eu^{3+} and 0.4, 4, 14, 18 μM Tb^{3+} in DMEM) for 12 h, 36 and 48 h, respectively, at 37 °C under 5% CO_2. Thereafter, MTT (20 μL, 5 mg/mL) was added to each well, and the plate was incubated for 4 h at 37 °C. After the addition of dimethyl sulfoxide (DMSO, 100 μL/well), the cell plate was allowed to stand at 37 °C for 15 min. The optical density was measured at 492 nm using a microplate reader (Shanghai Sanco Instrument Co., Ltd. 318C-microplate reader).

Fluorescence Microscopic Imaging. For Cu^{2+} imaging, BHK-21, A549, and HeLa cells were grown in DMEM supplemented with 10% FBS in an atmosphere of 5% CO_2 and 95% air at 37 °C humidified air for 24 h. Then the cultured BHK-21 and HeLa cells were incubated with **1** (40 μM Eu^{3+} and 4 μM Tb^{3+} in DMEM) for 1 h. Subsequently, the cells were incubated with 25 μM $CuCl_2$ for another 1 h, and the cells were washed with PBS three times to remove free **1** and ions before fluorescence imaging.

For target cell imaging, the cultured A549 and HeLa cells were incubated with **3** (4 μM Eu^{3+} and 0.4 μM Tb^{3+} in DMEM) for 1 h, and the cells were washed with PBS three times to remove free **3** before imaging. All confocal images were collected with a Leica TCS SP8 inverted epifluorescence/reflectance laser scanning confocal microscope. Excitation was at 335 ± 20 nm, and emission was at 515, 545, and 616 nm.

RESULTS AND DISCUSSION

Synthesis and Characterization of Hybrid 1. The synthesis process for the triple-emitting luminescent dumbbell-like Au−Fe_3O_4 NPs is presented in Scheme 1. The dumbbell-like Au−Fe_3O_4 NPs were prepared according to the literature.[41] The as-synthesized NPs coated with a layer of oleate and oleylamine, as shown by transmission electron microscopy (TEM; Figure 1A), were further functionalized by ligand exchange. Co-binding Tb(III) complex and Eu(III) complex on the Fe_3O_4 side were obtained by incubating Tb:**1b** and Eu:**1a** with newly synthesized Au−Fe_3O_4 NPs. FITC as a reference agent was anchored on the Au side by HS-PEG-NH-

DOI: 10.1021/acs.inorgchem.5b00610
Inorg. Chem. 2015, 54, 7725−7734

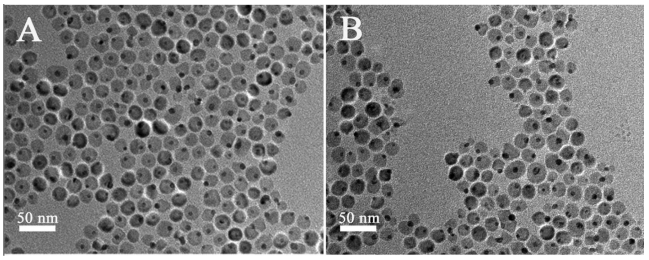

Figure 1. TEM images of (A) as-synthesized Au−Fe_3O_4 nanoparticles dispersed in hexane and (B) **1** dispersed in H_2O.

FITC (**1e**).[23] Hybrid **1** was readily dispersed in water and stayed for at least 2 weeks. TEM showed that there was no change in the morphology of the NPs during the ligand exchange process (Figure 1B). The hydrodynamic diameter of Au−Fe_3O_4 NPs was about 17 nm. However, after forming **1**, the hydrodynamic diameter was about 56 nm (Supporting Information Figure S3). The increase of the hydrodynamic size could be attributable to the binding of Tb:**1b** and Eu:**1a**. According to the Tb/Fe and Eu/Fe weight percentage (6.33% and 63.3%), about 393 Tb and 3933 Eu units are bound to each Au−Fe_3O_4 NP, corresponding to about 4326 ligands per Au−Fe_3O_4 NP.[33] Zeta potential measurement showed that **1c** and **1** served negative charge close to −3.95 mV ± 0.06 mV and −6.17 ± 0.15 mV, respectively. Also, the fluorescence intensity of **1** under a different time shows almost no change (Supporting Information Figure S4), which indicates that **1** is stable.

The FITC, Tb(III) complex, and Eu(III) complex coupling onto each Au−Fe_3O_4 particle was estimated by using a fluorescence spectrum. Figure 2 shows the emission spectrum

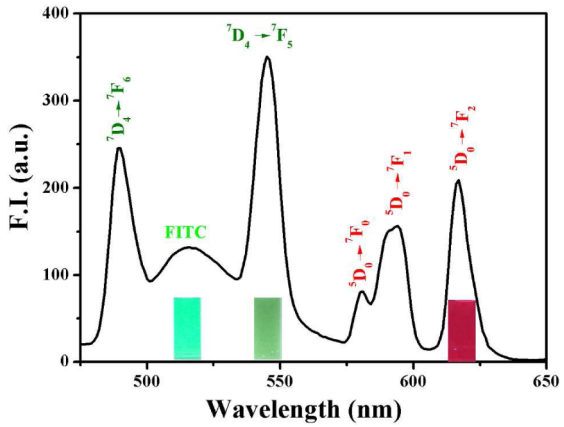

Figure 2. Fluorescence spectrum of **1** under excitation at 335 nm and corresponding fluorescence photographs of FITC, Tb:**1b**, and Eu:**1a** complexes.

of **1** under 335 nm excitation in Tris-HCl buffer (pH = 7.20). The hybrid **1** results in well-resolved triple fluorescence emission of FITC (515 nm), Tb^{3+} (490 and 545 nm) and Eu^{3+} (580, 593, and 616 nm), proving the FITC and the lanthanide complexes can be successfully linked to the particles. After FITC, Tb(III) complex and Eu(III) complex are chemically cobound onto the surface of Au−Fe_3O_4 NPs, the excitation and emission spectrum of the FITC and lanthanide complexes in the nanoparticles are not affected by the Au−Fe_3O_4 NPs, and the emissions of three fluorescent molecules are not negatively affected by one another. Vibrating sample magnetometer (VSM) measurements (Supporting Information Figure S5) proved that NPs had excellent superparamagnetism before and after modification. Compared with Au−Fe_3O_4 NPs, the saturation magnetization of **1** decreased from 39 to 14 emu g^{-1}, which was due to the increase of nonmagnetic portion in **1**. The FT-IR spectrum of oleic acid and oleylamine-coated Au−Fe_3O_4 NPs exhibited strong absorption bands at 2850 and 2915 cm^{-1}, which was attributed to symmetric and asymmetric C−H stretch of the oleyl chains, respectively.[23] After grafting the Tb(III) and Eu(III) complexes onto Au−Fe_3O_4 nanoparticles, the characteristic bands of oleic acid remarkably decreased, and a strong characteristic peak at 1597 cm^{-1} for ν_{as}(COO−) stretch vibrations was observed. Moreover, peak at 668 cm^{-1} corresponds to Fe−O absorption bands.[23] In addition, the peak at 1113 cm^{-1}, which is assigned to phenolic hydroxyl group vibration in Tb(III) and Eu(III) complexes, is not observed after forming Eu:AMC(Tb:cs124)-DTPA-PEG-Fe_3O_4-Au hybrid. However, a new absorption peak of C−O−Fe vibration at 1094 cm^{-1} appears, indicating that the phenolic hydroxyl group of Tb(III) and Eu(III) complexes are bound to the surface of Fe_3O_4 NPs.[45]

Binding Constant Study of Hybrid 1 to Cu^{2+}. In order to compare the binding constants of Tb:DTPA-cs124, Cu:DTPA-cs124, Eu:DTPA-AMC, and Cu:DTPA-AMC, the potentiometric titration was performed. First, according to the potentiometric titration V−pH curves (Supporting Information Figures S1A and S2A) and eq 1, the $\bar{n}_H$ was obtained.

$$\bar{n}_H = \frac{jC_L + C_A + [OH^-] - [Na^+] - [H^+]}{C_L} \quad (1)$$

Here j is the amount of H^+ in ligand acid H_jL, C_L is the concentration of H_jL, C_A is the concentration of strong acid, $[H^+]$ is obtained from pH value measured, $[OH^-]$ is obtained from the water constant of $K_W = [H^+][OH^-]$ at experimental temperature, and $[Na^+]$ is the concentration of NaOH in solution. Then, the protonation constants of DTPA-cs124 and DTPA-AMC were calculated on the basis of the Bjerrum's Half-$\bar{n}$ Method, the value of pH, and $\bar{n}$. The results were shown in Table 1. Finally, according to the potentiometric titration V−pH curves (Supporting Information Figures S1B,C and S2B,C) and eqs 2−4, the $\bar{n}$ was obtained.

$$\bar{n}_H = \frac{\beta_1^H[H^+] + 2\beta_2^H[H^+]^2 + \ldots + j\beta_j^H[H^+]^j}{1 + \beta_1^H[H^+] + \beta_2^H[H^+]^2 + \ldots + \beta_j^H[H^+]^j} \quad (2)$$

$$[L] = \frac{jC_L + C_A + [OH^-] - [Na^+] - [H^+]}{\beta_1^H[H^+] + 2\beta_2^H[H^+]^2 + \ldots + j\beta_j^H[H^+]^j} \quad (3)$$

$$\bar{n} = \frac{C_L - \frac{jC_L + C_A + [OH^-] - [Na^+] - [H^+]}{\bar{n}_H}}{C_M} \quad (4)$$

Here β_1^H, β_2^H, β_j^H are the cumulative protonation constants, and C_M is the concentration of metal ion analyzed. Finally, according to Bjerrum's Half-Method and the value of L and $\bar{n}$, the stability constants of complexes were calculated. As shown in Table 2, the binding constants of Cu:DTPA-cs124 ($K_{Cu:DTPA\text{-}cs124} = 10^{22.26}$) and Cu:DTPA-AMC ($K_{Cu:DTPA\text{-}AMC} = 10^{21.77}$) are higher than those of corresponding Tb:DTPA-cs124 ($K_{Tb:DTPA\text{-}cs124} = 10^{20.44}$) and Eu:DTPA-AMC ($K_{Eu:DTPA\text{-}AMC} = 10^{19.67}$).

DOI: 10.1021/acs.inorgchem.5b00610
Inorg. Chem. 2015, 54, 7725−7734

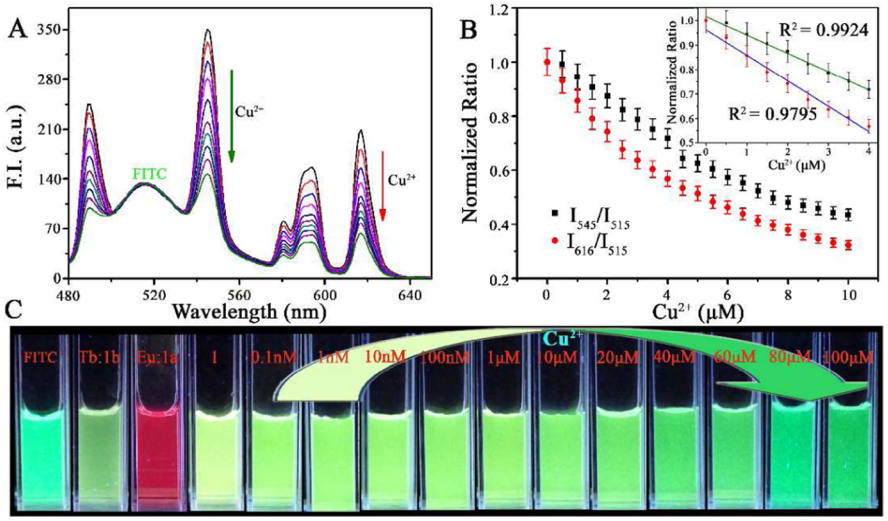

Figure 3. (A) Fluorescent spectra of **1** (3 μM Eu^{3+}, 0.3 μM Tb^{3+}) upon addition of Cu^{2+} from 0 μM to 10 μM in Tris-HCl buffer (50 mM, pH 7.20). (B) The normalized intensity changes of both 545 and 616 nm by comparing the intensity with and without Cu^{2+}. (C) The photographs of FITC, Tb:**1b**, and Eu:**1a** complexes and optical color response of **1** (16 μM Eu^{3+}, 1.6 μM Tb^{3+}) to the different concentrations of Cu^{2+} (from 0.1 nM to 100 μM) in Tris-HCl buffer (50 mM, pH 7.20). Excitation occurred at 335 nm.

Fluorescence Titration Detection of Cu^{2+}. A notable finding in this work was the high responsiveness of **1** to Cu^{2+}. Generally, single-intensity-based fluorescence sensors for Cu^{2+} ions are prone to errors because of unpredictable factors such as fluctuated light source intensity, instrumental drift, variations in excited sensors, probe concentration, biological background fluorescence, environmental conditions, and probe photobleaching.[30,31] In principle, these problems can be reduced by using ratiometric fluorescent probes, which can estimate the concentration of analyte and provide a built-in correction for environmental impact.[46,47] Recently, although some ratiometric fluorescent probes for copper ion have been synthesized in recent years,[48,49] most of them cannot work in aqueous solution. Furthermore, studies on the ratiometric imaging of Cu^{2+} in living cells are very rare.[50−53]

In order to get the detection conditions of optimization, the fluorescent intensities of **1** based on the replacement reaction between Eu^{3+}/Tb^{3+} and Cu^{2+} were measured at different time intervals. The results reveal that the response time of **1** to different concentrations of Cu^{2+} ion is fast and can reach equilibrium within 5 min (Supporting Information Figure S7). In addition, the fluorescent responses of **1** to Cu^{2+} ion at the different pH values were also investigated (Supporting Information Figure S8). We found that the changes of fluorescence intensity remained stable over pH from 5 to 11, indicating that this sensor could be employed to detect Cu^{2+} in a wide pH range. In our study, the subsequent experiments were performed in buffered solution at pH 7.2.

Figure 3A shows the emission spectrum of the aqueous solution containing **1** with different amounts of Cu^{2+}. Due to the replacement of Eu^{3+} and Tb^{3+} on the surface of the Fe_3O_4 by Cu^{2+}, the Tb(III) and Eu(III) emissions at 545 and 616 nm decrease gradually with increasing Cu^{2+} concentration. In contrast, the FITC emission at 515 nm is not changing with increasing Cu^{2+} concentration. Like fluorescence spectra, the same response signals also appear in the phosphorescence spectra (Supporting Information Figure S9). Figure 3B shows the correlation between the intensity ratio and the concentration of added Cu^{2+} ions, and the concentration of Cu^{2+} and emission intensity ratios (I_{615}/I_{515} and I_{545}/I_{515}) exhibit a good linear correlation. The detection limit (3σ/slope) based on the formation of Cu:DTPA-Fe_3O_4-Au-FITC was 30 nM. Such nanomolar detection limit is lower than those for the reported organic fluorophores[54] and the US EPA drinking water standard value of Cu^{2+} ions (1.3 ppm, 20 μM),[55] which indicates that probe **1** is sensitive for detection of Cu^{2+} in aqueous solutions. Hybrid **1** showed yellow luminescence in the absence of Cu^{2+} under UV illumination. However, with variation of the Cu^{2+} concentration, the yellow luminescence could be adjusted, and the NPs displayed a clear color change from yellow to green (Figure 3C) by the naked eye.

Mechanism for Probe 1 To Selectively Bind to Cu^{2+}. Scheme 1 shows the recognition mechanism of this nanoprobe for sensing Cu^{2+}. The Cu^{2+} replaced the lanthanide ions (Tb^{3+} and Eu^{3+}) and coordinated with carboxyl and amino of DTPA molecules, because the binding constants of Cu:DTPA-cs124 and Cu:DTPA-AMC are higher than those of the corresponding Tb:DTPA-cs124 and Eu:DTPA-AMC. In the presence of Cu^{2+}, the Eu^{3+} and Tb^{3+} ions of **1** were replaced by Cu^{2+}, forming a new Cu:AMC(Cu:cs124)-DTPA-PEG-Fe_3O_4-Au-HS-PEG-NH-FITC hybrid. Therefore, the Tb(III) and Eu(III) emissions at 545 and 616 nm decrease in the presence of the Cu^{2+}. In the above replaced process, the free Eu^{3+} and Tb^{3+} ions that were replaced in aqueous solution could be detected reversibly by cs124-DTPA-NH-PEG-DBA-Fe_3O_4-Au-PEG-NH-FITC (Supporting Information Figure S10). At the same time, cyclic voltammetry of the electrochemical method was used to clarify the sensing process. We test the electrode properties of Tb(III) and Eu(III) complexes in the absence and presence of Cu^{2+} in a three-electrode system using Pt as the auxiliary electrode, Hg/Hg_2SO_4 as the reference electrode, and 1 mol/L KCl solution as electrolyte. As shown in Supporting Information Figure S11, compared with those of Eu:**1a** and Tb:**1b**, the anodic (A) and cathodic (C) peak potentials of Eu:**1a** and Tb:**1b** upon adding Cu^{2+} obviously appeared and match with the free Cu^{2+} in the electrode solution in the range −0.6 to 1 V, indicating that the new Cu:**1a** and Cu:**1b** complexes were formed.

The quenching mechanism of **1** with increasing Cu^{2+} can be demonstrated by measuring the lifetimes of Eu(III) and Tb(III)

DOI: 10.1021/acs.inorgchem.5b00610
Inorg. Chem. 2015, 54, 7725−7734

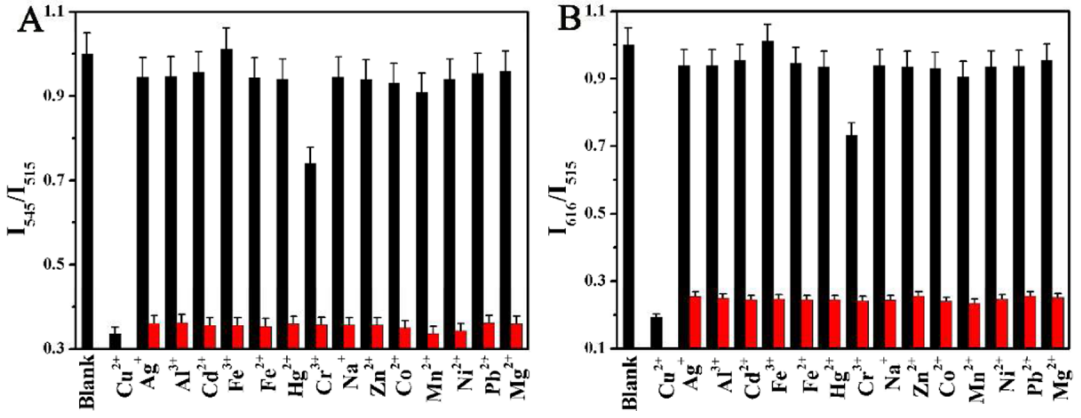

Figure 4. Normalized fluorescence responses of **1** (10 μM Eu^{3+}, 1 μM Tb^{3+}) to various metal ions (100 μM) with the final integrated ratiometric fluorescence response of (A) 545 nm over 515 nm and (B) 616 nm over 515 nm. Black bars represent the addition of the competing metal ion to the solution of **1**. Red bars represent the addition of Cu^{2+} to the solution containing the other metal and **1**.

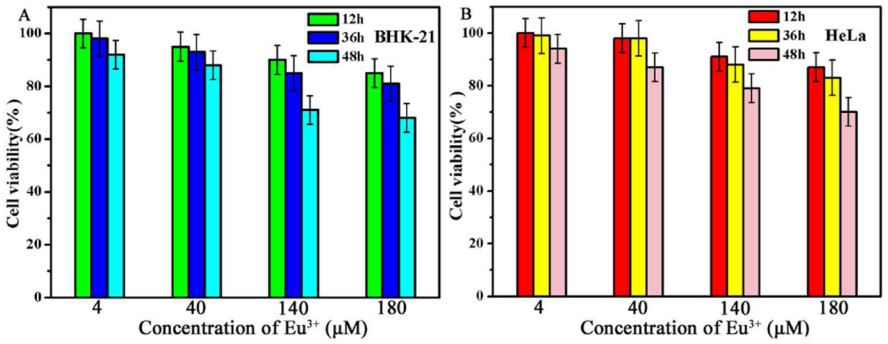

Figure 5. In vitro cell viability of BHK-21 (A) and HeLa (B) cells incubated with **1** with different concentrations (4, 40, 140, 180 μM Eu^{3+} and 0.4, 4, 14, 18 μM Tb^{3+}) incubated for 12, 36, and 48 h at 37 °C.

complexes in nanocomposite **1** in the absence and presence of Cu^{2+}.[56] The average lifetimes of Eu(III) and Tb(III) in nanocomposite **1** were 0.467 ms at 545 nm ($^5D_4$) and 0.727 ms at 616 nm ($^5D_0$), respectively (Supporting Information Table S1). After addition of Cu^{2+}, the average lifetimes of Eu(III) and Tb(III) in nanocomposite **1** decreased to 6.41 μs at 545 nm and 115.21 μs at 616 nm, respectively. The decreased lifetimes indicated that nanocomposite **1** interacted with Cu^{2+}, and the contents of Eu(III) and Tb(III) ions were decreased, resulting in fluorescent quenching. In addition, compared with the other detection system,[57−60] the longer fluorescence lifetime of nanocomposite **1** could completely decay to the various nonspecific fluorescence and eliminate the background emission from a biological matrix.

To demonstrate the selectivity of this three-channel ratiometric fluorescence sensor, several different metal ions including Ag^{+}, Al^{3+}, Co^{2+}, Mn^{2+}, Cd^{2+}, Hg^{2+}, Mg^{2+}, Na^{+}, Pb^{2+}, Zn^{2+}, Ni^{2+}, Fe^{2+}, Fe^{3+}, and Cr^{3+} at the same concentration of 100 μM were used to check their influence on the fluorescence characteristics (Figure 4 and Supporting Information Figure S12, black bars). It was found that only Cu^{2+} enormously decreases the I_{545}/I_{515} and I_{616}/I_{515} ratios, indicating the high selectivity of the ratiometric fluorescence sensor to Cu^{2+}. Moreover, competition experiments were performed by adding Cu^{2+} to solutions of **1** in the presence of other cations. As shown in Figure 4 (red bars), both in the absence and presence of other cations, significant quenching of fluorescence was observed for **1** upon addition of Cu^{2+}. The results were in accord with literature that Cu^{2+} had a higher binding constant than other metal ions in DTPA system.[61] We tested the interference of counterion such as Cl^{-}, SO_4^{2-}, NO_3^{-}, and CH_3COO^{-} (Supporting Information Figure S13). The experimental results indicated that the effects of counterion were the same. The results indicate that these commonly coexistent ions do not affect the sensing of Cu^{2+} by **1**. Thus, **1** can be used as a highly selective fluorescent probe for Cu^{2+}.

Cell Toxicity and Fluorescence Imaging of Sensing Cu^{2+} in Cells. Toxicity is a major factor to be considered in application of **1** to biological applications. To address this issue, the cytotoxicity of **1** was determined by cell culture using the BHK cells and HeLa cells as the tested cells. The MTT (3-(4,5-dimethylthiazol-2-yl)-2,5-diphenyltetrazolium bromide) assay was used to evaluate the viability of the BHK cells and HeLa cells after exposure to the hybrid NPs for 12, 36, and 48 h at various concentrations of NP (4, 40, 140, 180 μM Eu^{3+} and 0.4, 4, 14, 18 μM Tb^{3+}). As shown in Figure 5, the cell viabilities of both of the two cells were still greater than 68% after 48 h. While in the fluorescence imaging Cu^{2+}, the concentration of Eu^{3+} was 3 μM. Thus, **1** exhibits low toxicity on the cells and has good potential for practical imaging applications.

We further proceeded to investigate the suitability of our nanoprobe in multiplex monitoring Cu^{2+} in BHK cells and HeLa cells. BHK cells and HeLa cells were first incubated with **1** in a serum-supplemented cell culture medium for 1 h at 37 °C. It was discovered that the green (Figure 6A,I), yellow (Figure 6B,J), and red colors (Figure 6C,K) were clearly observed simultaneously under 335 ± 20 nm excitation, and the overlay signals were yellow-green color (Figure 6D,L).

DOI: 10.1021/acs.inorgchem.5b00610
Inorg. Chem. 2015, 54, 7725−7734

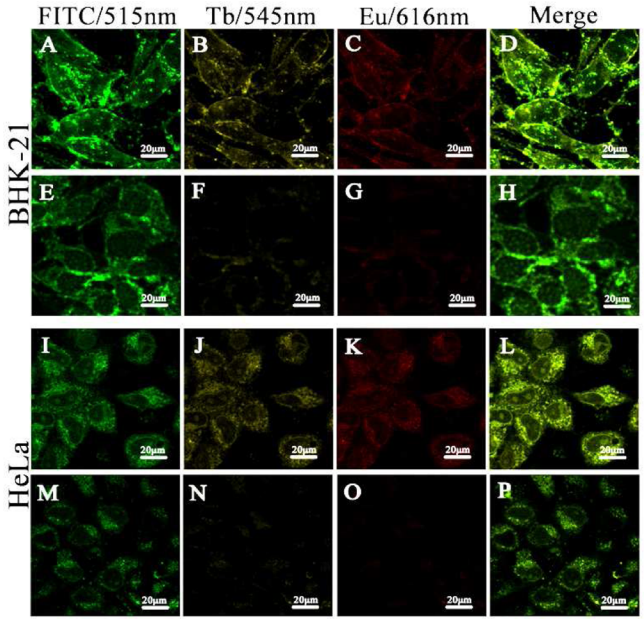

Figure 6. Confocal fluorescence images of BHK-21 cells (A–D) after incubation with **1** and (E–H) after addition of 25 μM Cu^{2+} to the **1** treated cells for 1 h and HeLa cells (I–L) after incubation with **1** and (M–P) after addition 25 μM Cu^{2+} to the **1** treated cells for 1 h. Excitation at 315–355 nm and emission at 515, 545, and 616 nm. (A, E and I, M) Fluorescence image of FITC (green); (B, F and J, N) fluorescence image of Tb(III) complex (yellow); (C, G and K, O) fluorescence image of Eu(III) complex (red); (D) overlay of A, B, and C; (H) overlay of E, F, and G; (L) overlay of I, J, and K; (P) overlay of M, N, and O.

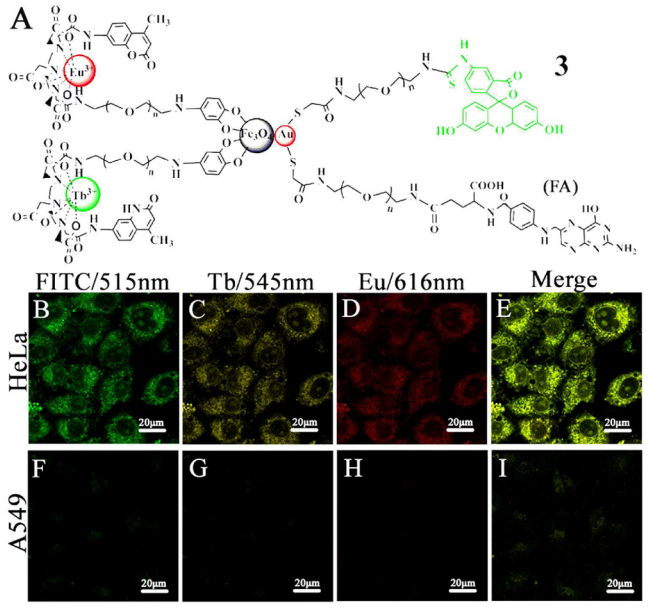

Figure 7. (A) Structure of folic acid labeled hybrid **3**. Confocal fluorescence images of HeLa cells (B–E) and A549 cells (F–I) after incubation with **3**. Excitation at 335 ± 20 nm and emission at 515, 545, and 616 nm. (B, F) Fluorescence image of FITC (green); (C, G) fluorescence image of Tb(III) complex (yellow); (D, H) fluorescence image of Eu(III) complex (red); (E) overlay of B, C, and D; (I) overlay of F, G, and H.

However, after addition of Cu^{2+} (25 μM) and being incubated for another 1 h, the yellow and red fluorescence signals were very dim (Figure 6F,N,G,O), while the green fluorescence remained very intense (Figure 6E,M), and the overlay signals were the main green color (Figure 6H,P), indicating the Cu^{2+} did not quench the fluorescence of FITC. The fluorescence images quenched a little as the concentration of Cu^{2+} decreased (see the Supporting Information, Figures S14 and S15). This implied that the fluorescence of Eu(III) and Tb(III) complexes was rapidly and substantially quenched by 25 μM Cu^{2+}, providing clear evidence of fluorescence quenching–ratiometric imaging of Cu^{2+} in living cells by the nanosensor. It should be cautioned that the long exposure to ultraviolet light is highly detrimental to cells in fluorescence imaging.

Target Cell Imaging of Folate-Labled Hybrid 3. To validate the use of **1** for multicolor imaging to folate receptor (FR)-overexpressing cells, **1** was further modified with HS-PEG-NH-FA (**1f**), and the obtained **3** (as shown in Figure 7A) was confirmed by UV–vis measurements (Supporting Information Figure S16). In the UV–vis spectra, two new absorbance bands at 283 and 370 nm, which are from FA, are observed in **3**, which indicates that **1f** has been grafted onto the surface of Au–Fe_3O_4 NPs. Compound **3** was tested as tools for multicolor imaging to FR-overexpressing cells. As shown in Figure 7, HeLa cells treated with **3** simultaneously displayed triple-color images with green (Figure 7B), yellow (Figure 7C), and red (Figure 7D) fluorescence signals under 335 ± 20 nm excitation, and the three fluorescence signals overlay resulted in yellow-green color (Figure 7E). In contrast, A549 cells incubated with **3** showed weak multicolor fluorescence (Figure 7F–I). These results indicate a high specific affinity between folate on **3** and folate receptors on the HeLa cells and weak interaction between **3** and folate receptor deficient A549 cells. These results clearly demonstrated that **3** could apply for multicolor in vitro imaging of the overexpressed folate receptors cells. TEM imaging about the location of nanoprobe and cell is demonstrated in Supporting Information Figure S17. After the same incubation time, both **1** and **3** internalized into the cytoplasm of HeLa cells (Supporting Information Figure S17A,B), and a small amount of **3** was able to enter the nucleus of cells (Supporting Information Figure S17B).[61–64]

CONCLUSIONS

We have demonstrated a simple strategy for the rational design of a ratiometric and triple-emitting probe based on incorporating lanthanide complexes and organic dyes onto Au–Fe_3O_4 NPs. The NPs exhibit distinguishable emission spectra with bands at 515, 545, and 616 nm by one single wavelength excitation, which were recorded to simultaneously and selectively detect the Cu^{2+} in aqueous solution with a detection limit of 30 nM. In addition, adjustment of Cu^{2+} concentrations allows fine-tuning of the fluorescent color along yellow, yellow-green, and green and extends to ratiometric imaging of Cu^{2+} in cells. Moreover, the folic-acid-labeled fluorescent nanoprobe enables targeted multicolor fluorescent imaging of FR-overexpressing HeLa cell lines in vitro. Generally, single-intensity-based probes are prone to errors due to unpredictable factors, such as biological background fluorescence, environmental conditions, and instrumental efficiency. Thus, this multicolor fluorescent imaging prevents false positive results caused by detection with a single fluorescent color. The strategy demonstrated here can be easily extended to other types of triple-emitting hybrid for ratiometric fluorescence sensing applications.

DOI: 10.1021/acs.inorgchem.5b00610
Inorg. Chem. 2015, 54, 7725–7734

■ ASSOCIATED CONTENT

Supporting Information

Hydrodynamic diameters of **1**, fluorescence spectra of **1** in Tris-HCl buffer (50 mM, pH 7.20) at different times, the saturated magnetization (M) of as-synthesized Au−Fe_3O_4 NPs and **1**, the FT-IR spetra of as-sythesized Au−Fe_3O_4 NPs, Eu:**1a**, Tb:**1b**, and **1c**. Phosphorescence spectra of **1** upon addition of Cu^{2+}. Cyclic voltammograms of Cu^{2+}, Eu^{3+}, Eu:**1a**, and Eu:**1a** reacting with Cu^{2+} in the electrode solution. Cyclic voltammograms of Cu^{2+}, Tb^{3+}, Tb:**1b**, and Tb:**1b** reacting with Cu^{2+} in the electrode solution. The Supporting Information is available free of charge on the ACS Publications website at DOI: 10.1021/acs.inorgchem.5b00610.

■ AUTHOR INFORMATION

Corresponding Authors

*E-mail: wangbd@lzu.edu.cn.
*E-mail: haotaichen@163.com.

Notes

The authors declare no competing financial interest.

■ ACKNOWLEDGMENTS

This work was supported by the National Natural Science Foundation of China (21271093, 21431002, and 21401091), the National Basic Research Program of China (973 Program) No. 2012CB933102, the Program for New Century Excellent Talents in University (NCET-13-0262), and the Fundamental Research Funds for the Central Universities (lzujbky-2014-k06).

■ REFERENCES

(1) Chatterjee, A.; Guo, J. T.; Lee, H. S.; Schultz, P. G. *J. Am. Chem. Soc.* **2013**, *135*, 12540−12543.
(2) Wang, F.; Liu, X. G. *Acc. Chem. Res.* **2014**, *47*, 1378−1385.
(3) Kwon, J. E.; Park, S.; Park, S. Y. *J. Am. Chem. Soc.* **2013**, *135*, 11239−11246.
(4) Wang, L.; Tan, W. H. *Nano Lett.* **2006**, *6*, 84−88.
(5) Kobayashi, H.; Koyama, Y.; Barrett, T.; Hama, Y.; Regino, C. A. S.; Shin, I. S.; Jang, B.−S.; Le, N.; Paik, C. H.; Choyke, P. L.; Urano, Y. *ACS Nano* **2007**, *1*, 258−264.
(6) Wilson, R.; Cossins, A. R.; Spiller, D. G. *Angew. Chem., Int. Ed.* **2006**, *45*, 6104−6117.
(7) Luo, F.; Zheng, L. Y.; Chen, S. S.; Cai, Q. H.; Lin, Z. Y.; Qiu, B.; Chen, G. N. *Chem. Commun.* **2012**, *48*, 6387−6389.
(8) Su, S.; Wei, X. P.; Zhong, Y. L.; Guo, Y. Y.; Su, Y. Y.; Huang, Q.; Lee, S.−T.; Fan, C. H.; He, Y. *ACS Nano* **2012**, *6*, 2582−2590.
(9) Akbulut, M.; Ginart, P.; Gindy, M. E.; Theriault, C.; Chin, K. H.; Soboyejo, W.; Prud'homme, R. K. *Adv. Funct. Mater.* **2009**, *19*, 718−725.
(10) Wu, J.; Ye, Z. Q.; Wang, G. L.; Jin, D. Y.; Yuan, J. L.; Guan, Y. F.; Piper, J. *J. Mater. Chem.* **2009**, *19*, 1258−1264.
(11) Nishiyabu, R.; Hashimoto, N.; Cho, T.; Watanabe, K.; Yasunaga, T.; Endo, A.; Kaneko, K.; Niidome, T.; Mureta, M.; Adachi, C.; Katayama, Y.; Hashizume, M.; Kimizuka, N. *J. Am. Chem. Soc.* **2009**, *131*, 2151−2158.
(12) Bae, S. W.; Tan, W. H.; Hong, J.−I. *Chem. Commun.* **2012**, *48*, 2270−2282.
(13) Gomes, M. C.; Fernandes, R.; Cunha, Â.; Tomé, J. P. *J. Mater. Chem. B* **2013**, *1*, 5429−5435.
(14) Wang, X.; Xia, Y. Q.; Liu, Y. Y.; Qi, W. X.; Sun, Q. Q.; Zhao, Q.; Tang, B. *Chem. - Eur. J.* **2012**, *18*, 7189−7195.
(15) Lewis, D. J.; Day, T. M.; MacPherson, J. V.; Pikramenou, Z. *Chem. Commun.* **2006**, 1433−1435.
(16) Elmes, R. B. P.; Orange, K. N.; Cloonan, S. M.; Williams, D. C.; Gunnlaugsson, T. *J. Am. Chem. Soc.* **2011**, *133*, 15862−15865.
(17) Truman, L. K.; Comby, S.; Gunnlaugsson, T. *Angew. Chem., Int. Ed.* **2012**, *51*, 9624−9627.
(18) Comby, S.; Gunnlaugsson, T. *ACS Nano* **2011**, *5*, 7184−7197.
(19) Wang, B. D.; Hai, J.; Wang, Q.; Li, T. R.; Yang, Z. Y. *Angew. Chem., Int. Ed.* **2011**, *50*, 3063−3066.
(20) Yang, C.; Wu, J. J.; Hou, Y. L. *Chem. Commun.* **2011**, *47*, 5130−5141.
(21) Liu, Z. C.; Li, B.; Wang, B. D.; Yang, Z. Y.; Wang, Q.; Li, T. R.; Qin, D. D.; Li, Y.; Wang, M. F.; Yan, M. H. *Dalton Trans.* **2012**, *41*, 8723−8728.
(22) Wu, W.; Hao, R.; Liu, F.; Su, X. T.; Hou, Y. L. *J. Mater. Chem. A* **2013**, *1*, 6888−6894.
(23) Liu, J.; Zhang, W.; Zhang, H. L.; Yang, Z. Y.; Li, T. R.; Wang, B. D.; Huo, X.; Wang, R.; Chen, H. T. *Chem. Commun.* **2013**, *49*, 4938−4940.
(24) Wang, L.; Yang, C.; Tan, W. H. *Nano Lett.* **2005**, *5*, 37−43.
(25) Ishow, E.; Brosseau, A.; Clavier, G.; Nakatani, K.; Tauc, P.; Debuisschert, C. F.; Neveu, S.; Sandre, O.; Léaustic, A. *Chem. Mater.* **2008**, *20*, 6597−6599.
(26) Bünzli, J. C. G.; Eliseeva, S. V. *Chem. Sci.* **2013**, *4*, 1939−1949.
(27) dos Santos, C. M. G.; Harte, A.; Quinn, S. J.; Gunnlaugsson, T. *Coord. Chem. Rev.* **2008**, *252*, 2512−2527.
(28) Pershagen, E.; Nordholm, J.; Borbas, K. E. *J. Am. Chem. Soc.* **2012**, *134*, 9832−9835.
(29) Feng, J.; Zhang, H. J. *Chem. Soc. Rev.* **2013**, *42*, 387−410.
(30) Comby, S.; Surender, E. M.; Kotova, O.; Truman, L. K.; Molloy, J. K.; Gunnlaugsson, T. *Inorg. Chem.* **2014**, *53*, 1867−1869.
(31) McMahon, B. K.; Gunnlaugsson, T. *J. Am. Chem. Soc.* **2012**, *134*, 10725−10728.
(32) Xu, C. J.; Xie, J.; Ho, D.; Wang, C.; Kohler, N.; Walsh, E. G.; Morgan, J. R.; Chin, Y. E.; Sun, S. H. *Angew. Chem., Int. Ed.* **2008**, *47*, 173−176.
(33) Xu, C. J.; Wang, B. D.; Sun, S. H. *J. Am. Chem. Soc.* **2009**, *131*, 4216−4217.
(34) Lyon, J. L.; Fleming, D. A.; Stone, M. B.; Schiffer, P.; Williams, M. E. *Nano Lett.* **2004**, *4*, 719−723.
(35) Waggoner, D. J.; Bartnikas, T. B.; Gitlin, J. D. *Neurobiol. Dis.* **1999**, *6*, 221−230.
(36) Turel, M.; Duerkop, A.; Yegorova, A.; Scripinets, Y.; Lobnik, A.; Samec, N. *Anal. Chim. Acta* **2009**, *644*, 53−60.
(37) Kessler, M. A. *Anal. Chim. Acta* **1998**, *364*, 125−129.
(38) Chen, X. L.; Estévez, M. C.; Zhu, Z.; Huang, Y. F.; Chen, Y.; Wang, L.; Tan, W. H. *Anal. Chem.* **2009**, *81*, 7009−7014.
(39) Lei, J. Y.; Wang, L. Z.; Zhang, J. L. *ACS Nano* **2011**, *5*, 3447−3455.
(40) Tremblay, M. S.; Halim, M.; Sames, D. *J. Am. Chem. Soc.* **2007**, *129*, 7570−7577.
(41) Yu, H.; Chen, M.; Rice, P. M.; Wang, S. X.; White, R. L.; Sun, S. H. *Nano Lett.* **2005**, *5*, 379−382.
(42) Wang, Y. M.; Cheng, T. H.; Liu, G. C.; Sheu, R. S. *J. Chem. Soc., Dalton Trans.* **1997**, *6*, 833−837.
(43) Aronov, O.; Horowitz, T.; Gabizon, A.; Gibson, D. *Bioconjugate Chem.* **2003**, *14*, 563−574.
(44) Bjerrum, J. *Metal Ammine Formation in Aqueous Solution*; Haase: Copenhagen, 1941.
(45) Cotton, F. A. Wilkinson, G. *Advanced Inorganic Chemistry*; Interscience Publishers: London, 1974.
(46) Liu, B.; Wang, J. F.; Ge, Z.; Bai, R. K.; Pang, Y. *ACS Appl. Mater. Interfaces* **2014**, *6*, 4402−4407.
(47) Liu, Y.; Yu, D. H.; Ding, S. S.; Xiao, Q.; Jun, G.; Feng, G. Q. *ACS Appl. Mater. Interfaces* **2014**, *6*, 17543−17550.
(48) Kumari, N.; Dey, N.; Jha, S.; Bhattacharya, S. *ACS Appl. Mater. Interfaces* **2013**, *5*, 2438−2445.
(49) Lan, M. H.; Zhang, J. F.; Chui, Y.-S.; Wang, P. F.; Chen, X. F.; Lee, C.-S.; Kwong, H.-L.; Zhang, W. J. *ACS Appl. Mater. Interfaces* **2014**, *6*, 21270−21278.
(50) Song, Z. G.; Kwok, R. T. K.; Zhao, E. G.; He, Z. K.; Hong, Y. N.; Lam, J. W. Y.; Liu, B.; Tang, B. Z. *ACS Appl. Mater. Interfaces* **2014**, *6*, 17245−17254.

DOI: 10.1021/acs.inorgchem.5b00610
Inorg. Chem. 2015, 54, 7725−7734

(51) Liu, X. J.; Zhang, N.; Bing, T.; Shangguan, D. H. *Anal. Chem.* **2014**, *86*, 2289−2296.
(52) Chen, Y. C.; Zhu, C. C.; Cen, J. J.; Li, J.; He, W. J.; Jiao, Y.; Guo, Z. J. *Chem. Commun.* **2013**, *49*, 7632−7634.
(53) Zhu, A. H.; Qu, Q.; Shao, X. L.; Kong, B.; Tian, Y. *Angew. Chem., Int. Ed.* **2012**, *51*, 7185−7189.
(54) Wang, D. P.; Shiraishi, Y.; Hirai, T. *Chem. Commun.* **2011**, *47*, 2673−2675.
(55) Shiraishi, Y.; Tanaka, K.; Hirai, T. *ACS Appl. Mater. Interfaces* **2013**, *5*, 3456−3463.
(56) You, Y.; Han, Y.; Lee, Y.−M.; Park, S. Y.; Nam, W.; Lippard, S. J. *J. Am. Chem. Soc.* **2011**, *133*, 11488−11491.
(57) Li, M.; Selvin, P. R. *Bioconjugate Chem.* **1997**, *8*, 127−132.
(58) McCranor, B. J.; Szmacinski, H.; Zeng, H. H.; Stoddard, A. K.; Hurst, T.; Fierke, C. A.; Lakowicz, J. R.; Thompson, R. B. *Metallomics* **2014**, *6*, 1034−1042.
(59) Yu, J. B.; Sun, L.; Peng, H. H.; Sticha, M. I. J. *J. Mater. Chem.* **2010**, *20*, 6975−6981.
(60) Santos, C. M. G.; Gunnlaugsson, T. *Dalton Trans.* **2009**, 4712−4721.
(61) Paul-Roth, C.; Raymond, K. N. *Inorg. Chem.* **1995**, *34*, 1408−1412.
(62) Dobrovolskaia, M. A.; McNeil, S. E. *Nat. Nanotechnol.* **2007**, *2*, 469−478.
(63) Porter, A. E.; Gass, M.; Muller, K.; Skepper, J. N.; Midgley, P. A.; Welland, M. *Nat. Nanotechnol.* **2007**, *2*, 713−717.
(64) Wang, Y. L.; Wang, J.; Deng, X.; Wang, J.; Wang, H.; Wu, M.; Jiao, Z.; Liu, Y. *Nano Res.* **2009**, *2*, 543−552.

DOI: 10.1021/acs.inorgchem.5b00610
Inorg. Chem. 2015, 54, 7725−7734